Inorg. Chem. **2007**, *46*, 10372–10382

Solid-State Synthesis of Monazite-type Compounds Containing Tetravalent Elements

Damien Bregiroux,*[,†,‡] Olivier Terra,[§] Fabienne Audubert,[†] Nicolas Dacheux,[§] Virgine Serin,[||] Renaud Podor,[⊥] and Didier Bernache-Assollant[#]

Commissariat à l'Énergie Atomique, DEN/DEC/SPUA/LTEC, Cadarache, 13108 Saint Paul Lez Durance, France, Laboratoire Science des Procédés Céramiques et de Traitements de Surface, UMR-CNRS n°6638, 123 avenue Albert Thomas, 87060 Limoges, France, Groupe de Radiochimie, Institut de Physique Nucléaire d'Orsay, Université Paris-Sud-11, 91406 Orsay, France, Groupe Nanomatériaux, Centre d'Elaboration de Matériaux et d'Etudes Structurales, 29 rue Jeanne Marvig, BP 94347, 31055 Toulouse, France, Laboratoire de Chimie du Solide Minéral, UMR-CNRS 7555, Université Henri Poincaré Nancy I, BP 239, 54506 Vandoeuvre lès Nancy, France, and École Nationale Supérieure des Mines, CIS, 158 cours Fauriel, 42023 Saint Etienne, France

Received June 21, 2007

On the basis of optimized grinding/heating cycles developed for several phosphate-based ceramics, the preparation of brabantite and then monazite/brabantite solid solutions loaded with tetravalent thorium, uranium, and cerium (as a plutonium surrogate) was examined versus the heating temperature. The chemical reactions and transformations occurring when heating the initial mixtures of AnO_2/CeO_2, $CaHPO_4 \cdot 2H_2O$ (or CaO), and $NH_4H_2PO_4$ were identified through X-ray diffraction (XRD) and thermogravimetric/differential thermal analysis experiments. The incorporation of thorium, which presents only one stabilized oxidation state, occurs at 1100 °C. At this temperature, all the thorium–brabantite samples appear to be pure and single phase as suggested by XRD, electron probe microanalyses, and μ-Raman spectroscopy. By the same method, tetravalent uranium can be also stabilized in uranium–brabantite, i.e., $Ca_{0.5}U_{0.5}PO_4$, after heating at 1200 °C. Both brabantites, $Ca_{0.5}Th_{0.5}PO_4$ and $Ca_{0.5}U_{0.5}PO_4$, begin to decompose when increasing the temperature to 1400 and 1300 °C, respectively, leading to a mixture of CaO and AnO_2 by the volatilization of P_4O_{10}. In contrast to the cases of thorium and uranium, cerium(IV) is not stabilized during the heating treatment at high temperature. Indeed, the formation of $Ca_{0.5}Ce_{0.5}PO_4$ appears impossible, due to the partial reduction of cerium(IV) into cerium(III) above 840 °C. Consequently, the systems always appear polyphase, with compositions of $Ce^{III}_{1-2x}Ce^{IV}_xCa_xPO_4$ and $Ca_2P_2O_7$. The same conclusion can be also given when discussing the incorporation of cerium(IV) into $La_{1-2x}Ce^{III}_{x-y}Ce^{IV}_yCa_y(PO_4)_{1-x+y}$. This incomplete incorporation of cerium(IV) confirms the results obtained when trying to stabilize tetravalent plutonium in $Ca_{0.5}Pu^{IV}_{0.5}PO_4$ samples.

1. Introduction

In the framework of the French research law related to the specific conditioning of long-life radionuclides in dedicated ceramics, phosphate matrices were extensively studied.[1−5] On the basis of several properties of interest such as weight loading,[6] sintering capability,[7,8] and resistance to aqueous

* To whom correspondence should be addressed. E-mail: damien.bregiroux@ccr.jussieu.fr. Tel: +33 144274770. Fax: +33 144272548. Present address: Université Pierre et Marie Curie, Paris 6, CNRS UMR 7574, Chimie de la Matière Condensée de Paris, 4 place Jussieu, Paris F-75005, France.

† Commissariat à l'Énergie Atomique, DEN/DEC/SPUA/LTEC.

‡ Laboratoire Science des Procédés Céramiques et de Traitements de Surface.

§ Université Paris-Sud-11.

|| Centre d'Elaboration de Matériaux et d'Etudes Structurales.

⊥ Université Henri Poincaré Nancy I.

École Nationale Supérieure des Mines.

(1) Bregiroux, D.; Audubert, F.; Charpentier, T.; Sakellariou, D.; Bernache-Assollant, D. *Solid State Sci.* **2007**, *9*, 432−439.
(2) Terra, O.; Audubert, F.; Dacheux, N.; Guy, C.; Podor, R. *J. Nucl. Mater.* **2006**, *354*, 49−65.
(3) Terra, O.; Audubert, F.; Dacheux, N.; Guy, C.; Podor, R. *J. Nucl. Mater.* **2007**, *366*, 70−86.
(4) Clavier, N.; Dacheux, N.; Podor, R. *Inorg. Chem.* **2006**, *45*, 220−229.
(5) Dacheux, N.; Clavier, N.; Robisson, A. C.; Terra, O.; Audubert, F.; Lartigue, J. E.; Guy, C. *C. R. Acad. Sci.* **2004**, *7*, 1141−1152.
(6) Boatner, L. A.; Beall, G. W.; Abraham, M. M.; Finch, C. B.; Hurray, P. G.; Rappaz, M. In *Scientific Basis for Nuclear Waste Management*; Northrup, C. J. M., Jr., Ed.; New York, 1980; Vol. 2, p 289.

10.1021/ic7012123 CCC: $37.00
Published on Web 10/27/2007

alteration[8−11] or to radiation damage,[12−16] monazites ($M^{III}PO_4$), brabantites ($M^{II}_{0.5}M^{IV}_{0.5}PO_4$), and associated monazite/brabantite solid solutions ($M^{III}_{1-2x}M^{II}_xM^{IV}_xPO_4$) were selected for advanced types of experiments by the French Research Group NOMADE (CNRS/CEA/AREVA/EDF/French universities) in the so-called field of "technical feasibility".[17] The synthesis of monazites, especially in regards to the preparation[1,18−20], the process,[21−24] or the optimization of specific properties required,[9,16] has already been described. On the basis of their redox properties, the actinides considered for the development of such matrices could be mainly trivalent (Pu, Am, Cm) or tetravalent (Th, U, Np, Pu). This shows the reason for the interest in designing matrices which could accept both tri- and tetravalent elements in their structure, e.g., $M^{III}_{1-2x}M^{II}_xM^{IV}_xPO_4$.[5,7]

From a geochemical point of view, monazite ($LnPO_4$, with Ln = La−Tb) is the most abundant lanthanide phosphate observed in natural samples.[25] Such minerals appear as the major thorium source on earth, especially in several ores which are up to 14.3 and 15.6 wt % in ThO_2 and UO_2, respectively.[26,27] Some other observations revealed the presence of samples containing up to 50 wt % of thorium and the consequent lack of indication of the presence of lanthanides in the minerals.[25,28,29] The incorporation of both tetravalent elements in the "monazite structure" of natural minerals was usually explained by the following two coupled substitutions:

$$2Ln^{3+} \Leftrightarrow (Th,U)^{4+} + Ca^{2+} \quad (1)$$

$$Ln^{3+} + PO_4^{3-} \Leftrightarrow (Th,U)^{4+} + SiO_4^{4-} \quad (2)$$

Some analyses carried out on natural samples revealed that the mechanism described by eq 1 is widely predominant.[30−32] It leads to a complete and ideal solid solution $M^{III}_{1-2x}M^{II}_xM^{IV}_xPO_4$, between pure monazite and pure brabantite ($M^{II}_{0.5}M^{IV}_{0.5}PO_4$).[31] van Emden et al. also noted that in several samples containing cerium, the (Ca + Si) content was higher than that of (Th + U),[32] leading to the conclusion that tetravalent cerium was probably incorporated in the monazite structure through both coupled substitutions. However, no analysis was carried out to validate this hypothesis. In the field of the second coupled substitution (eq 2), one of the $ThSiO_4$ forms (huttonite) is isostructural from $LaPO_4$ (monoclinic system, space group $P2_1/n$), which is not the case for $USiO_4$ (tetragonal system, space group $I4_1/amd$). It is worth noting that $ThSiO_4$ could exist in both crystallographic forms,[33] with the phase transition from tetragonal to monoclinic occurring at about 1200 °C. Moreover, $USiO_4$ is unstable at temperatures higher than 500 °C in air (1 atm) and decomposes into UO_2 and SiO_2.[34,35]

The preparation of synthetic actinide-bearing monazites was driven by either wet or dry chemistry methods. Among the methods based on wet chemistry processes, a large section of the method involved the precipitation of initial crystallized precursors (e.g., rhabdophanes of formula $LnPO_4 \cdot {}^1/_2H_2O$),[36] then heat treatment above 700 °C.

For trivalent actinides, these methods allowed the preparation of $AnPO_4$ (with An = U, Pu, Am−Bk). The incorporation of trivalent uranium, which appears rather curious from a redox point of view, was obtained in anoxic conditions and in the presence of formic acid from a mixture of Na_3PO_4 and trivalent uranium solution.[37] The preparation of $PuPO_4$ was reported from $PuPO_4 \cdot {}^1/_2H_2O$ precipitated between 75 and 90 °C from a mixture of trivalent plutonium and phosphoric acid in the presence of concentrated sulfuric acid or from a mixture of plutonium trichloride and $(NH_4)_2HPO_4$.[38,39] After heating above 950 °C, this blue well-crystallized precursor was fully transformed into plutonium−monazite.[39,40] More recently, the preparation of $La_{1-x}Am_xPO_4$

(7) Terra, O.; Dacheux, O.; Audubert, F.; Podor, R. *J. Nucl. Mater.* **2006**, *352*, 224−232.
(8) Terra, O.; Clavier, N.; Dacheux, N.; Podor, R. *New J. Chem.* **2003**, *27*, 957−967.
(9) Poitrasson, F.; Oelkers, E. H.; Schott, J.; Montel, J.-M. *Geochim. Cosmochim. Acta* **2004**, *68*, 2207−2221.
(10) Oelkers, E. H.; Poitrasson, F. *Chem. Geol.* **2002**, *191*, 73−87.
(11) Cetiner, Z. S.; Wood, S. A.; Gammons, C. H. *Chem. Geol.* **2005**, *217*, 147−169.
(12) Ewing, R. C.; Haaker, R. F. *Nucl. Chem. Waste Manage.* **1980**, *1*, 51−57.
(13) Karioris, F. G.; Appaji Gowda, K.; Cartz, L. *Radiat. Eff. Lett.* **1981**, *58* (*1*−*2*), 1−3.
(14) Meldrum, A.; Boatner, L. A.; Weber, W. J.; Ewing, R. C. *Geochim. Cosmochim. Acta* **1998**, *62*, 2509−2520.
(15) Burakov, B. E.; Yagovkina, M. A.; Garbuzov, V. M.; Kitsay, A. A.; Zirlin, V. A. *Mater. Res. Soc. Symp. Proc.* **2004**, *824*, 219−224.
(16) Bregiroux, D.; Belin, R.; Valenza, P.; Audubert, F.; Bernache-Assollant, D. *J. Nucl. Mater.* **2007**, *366*, 52−57.
(17) Deschanels, X. *Evaluation de la Faisabilité Technique des Nouvelles Matrices de Conditionnement des Radionucléides à Vie Longue*; Technical Report DTCD/2004/5; Commissariat à l'Energie Atomique (CEA)-Département d'Etudes du Traitement et du Conditionnement des Déchets (DTCD): Paris, 2004.
(18) Su, M. Z.; Zhou, J.; Shao, K.-S. *J. Alloys Compd.* **1994**, *207*−*208*, 406−408.
(19) Onoda, H.; Nariai, H.; Maki, H.; Motooka, I. *Mater. Chem. Phys.* **2002**, *73*, 19−23.
(20) Hikichi, Y. *Mineral. J.* **1991**, *15*, 268−275.
(21) Hikichi, Y.; Nomura, T.; Tanimura, Y.; Suzuki, S. *J. Am. Ceram. Soc.* **1990**, *73*, 3594−3596.
(22) Hikichi, Y.; Ota, T. *Phosph. Res. Bull.* **1996**, *6*, 175−178.
(23) Bregiroux, D.; Lucas, S.; Champion, E.; Audubert, F.; Bernache-Assollant, D. *J. Eur. Ceram. Soc.* **2006**, *26*, 279−287.
(24) Bregiroux, D.; Audubert, F.; Bernache-Assollant, D. *Adv. Sci. Tech.* **2006**, *45*, 633−638.
(25) Förster, H. J. *Am. Mineral.* **1998**, *83*, 259−272.
(26) Gramaccioli, C. M.; Segalstad, T. M. *Am. Mineral.* **1978**, *63*, 757−761.
(27) Boatner, L. A. In *Rev. Mineral. Chem.* **2002**, *48*, 87−121.
(28) Montel, J. M.; Kornprobst, J.; Vielzeuf, D. *J. Metamorph. Geol.* **2000**, *3*, 335−342.
(29) Foerster, H. J.; Harlov, D. E. *Mineral. Mag.* **1999**, *63*, 587−594.
(30) Kucha, H. *Mineral. Mag.* **1980**, *43*, 1031−1034.
(31) Rose, R. *N. Jb. Miner. Mh.* **1980**, *H*(*6*), 247−257.
(32) Van Emden, B.; Thornber, M. R.; Graham, J.; Lincoln, F. J. *Can. Mineral.* **1997**, *35*, 95−104.
(33) Mazeina, L.; Ushakov, S. V.; Navrotsky, A.; Boatner, L. A. *Geochim. Cosmochim. Acta* **2005**, *69*, 4675−4683.
(34) Hoekstra, H. R.; Fuchs, L. H. *Science* **1956**, *123*, 105.
(35) Fuchs, L. H.; Hoekstra, H. R. *Am. Mineral.* **1959**, *44*, 1057−1063.
(36) Lucas, S.; Champion, E.; Bregiroux, D.; Bernache-Assollant, D.; Audubert, F. *J. Solid State Chem.* **2004**, *177*, 1302−1311.
(37) Drozdzynski, J. *Inorg. Chim. Acta* **1979**, *32*, L83−L85.
(38) Bamberger, C. E.; Haire, R. G.; Hellwege, H. E.; Begun, G. M. *J. Less-Common Met.* **1984**, *97*, 349−356.
(39) Bjorklund, C. W. *J. Am. Chem. Soc.* **1958**, *79* (24), 6347−6350.
(40) Cleveland, J. M. In *The Chemistry of Plutonium*; Gordon & Breach Science Publishers: New York, 1970.

with large amounts of ^{241}Am was reported by Aloy et al.[41] from associated precipitated rhabdophanes. The same method was finally applied to prepare amercium−monazite samples from amercium−rhabdophane,[42,43] at the gram scale, and $CmPO_4$,[44,45] $BkPO_4$, $CfPO_4$, and $EsPO_4$ at the microgram scale.[45] The main conclusion is that, excepted for uranium−monazite, which the preparation of remains doubtful due to the low stability of the trivalent oxidation state of uranium, actinide−monazite samples can be obtained easily from plutonium to einsteinium by using wet chemistry methods.

In contrast, some other actinides (Th, Pa, Np) cannot be incorporated in their trivalent oxidation state in the monazite structure. This requires their incorporation because of a coupled substitution, as described in eqs 1 and 2. Moreover, brabantites and monazite/brabantite solid solutions are rather difficult to obtain through wet chemistry methods. In this field, Podor et al. synthesized several single crystals of $La_{1-2x}Ca_xAn_xPO_4$ solid solutions (with An(IV) = Th, U) from mixtures of $La(OH)_3$, $Ca(OH)_2$ or CaO, $An(OH)_4$ or AnO_2, and concentrated phosphoric acid in hydrothermal conditions near those ofgeological conditions ($t = 24$ h, $T = 780$ °C, $P = 200$ MPa, Ni/NiO buffer to control the dioxygen fugacity and to avoid the oxidation of uranium(IV) into uranyl).[46,47] Only by this method were polyphase systems composed of $Ca_{0.5}U_{0.5}PO_4$ and $U_2(PO_4)(P_3O_{10})$[48] prepared, leading to the same conclusions given by Muto et al.[49]

According to the literature, single crystals of monazite and monazite/brabantite solid solutions were usually prepared by the flux method from a mixture of rare-earth oxide and lead diphosphate at 1300 °C.[50] The crystals of monazite (or monazite/brabantite) formed during the cooling step (975 °C $\leq T \leq$ 1300 °C) were finally isolated by the preferential dissolution of PbP_2O_7 in hot concentrated nitric acid. Several authors reported the formation of samples doped with uranium (up to 10 wt %), neptunium (3.0 wt %), plutonium (6.0 wt %), americium (up to 0.5 wt %), or curium (0.1 wt %).[6,51,52] While the formation of Am- or Cm-doped monazite samples is not surprising taking into account the stabilization of the trivalent oxidation state of these actinides, the incorporation of the two tetravalent actinides (U, Np) in monazite samples could not be explained by the formation of vacancies on the basis of the weight loadings considered. It probably involves the formation of $Ln_{1-2x}Pb_xAn_xPO_4$ solid solutions as an explanation of such weight loadings with tetravalent actinides.[53] For Pu-doped samples, the stabilization of both oxidation states could be also proposed[38,39,54] even though the probability of the presence of Pu(III) appears to be more important on the basis of the reduction of Pu(IV) into Pu(III), as already discussed in the literature.[55,56]

Consequently, the incorporation of high weight loadings of tetravalent actinides in the monazite structure requires one of the two coupled substitutions discussed in eqs 1 and 2.[57] This incorporation, which appears difficult to reach by wet chemistry methods, seems to occur only when considering dry chemistry methods. Indeed, samples of $Ca_{0.5}An_{0.5}PO_4$ (An = Th, U, Np) were prepared as single-phase samples after heating a mixture of AnO_2, $CaCO_3$, and $(NH_4)_2HPO_4$ at high temperature under inert conditions.[58] Orlova et al. prepared $Ca_{1/3}Gd_{1/3}Th_{1/3}PO_4$ by the thermal treatment of oxides mixture.[59] Tabuteau et al. reported the formation of $Ca_{0.5}Np_{0.35}Pu_{0.15}PO_4$ through the simultaneous incorporation of tetravalent neptunium and plutonium.[58] According to some recent experiments, samples of $Pu^{III}_{0.4}Pu^{IV}_{0.3}Ca_{0.3}PO_4$ monazite/brabantite solid solution were also obtained at high temperature.[16] In contrast, the application of the same procedure to the preparation of $Ca_{0.5}Pu_{0.5}PO_4$ remained unsuccessful, probably due to the reduction of Pu(IV) into Pu(III) during the heating treatment, leading to the formation of $PuPO_4$.[58] The same conclusion was given on the basis of several attempts to stabilize tetravalent cerium as $Ca_{0.5}Ce_{0.5}PO_4$. Heindl et al. used the high-temperature solid-state route to synthesize $M^{II}_{0.5}Ce^{IV}_{0.5}PO_4$ (with M^{II} = Ca, Ba, Sr).[60] All the resulting powders were green colored, as also observed by Orlova et al.[61] Moreover, the X-ray diffraction (XRD) lines exhibited a shift toward the small 2θ angles compared to the diagram of $CePO_4$ which is not in agreement with the fact the $^1/_2(Ce^{IV} + Ca^{II})$ couple is smaller than Ce^{III}. More recently, Pepin et al. performed the same experiment but observed neither green color nor shift in the XRD lines. They also noted the presence of a secondary phase, $Ca_2P_2O_7$.[62] The relationship between the Ca content and the powder color of $(Ce,Ca)PO_4$ was recently used by Imanaka et al. and Sivakumar et al. for the elaboration of green pig-

(41) Aloy, A. S.; Kovarskaya, E. N.; Koltsova, T. I.; Samoylov, S. E. In *Radioactive Waste Management and Environmental Remediation;* ASME, 2001.
(42) Keller, C.; Walter, K. H. *J. Inorg. Nucl. Chem.* **1965**, *27*, 1253−1260.
(43) Rai, D.; Felmy, A. R.; Fulton, R. W. *Radiochim. Acta* **1992**, *56*, 7−14.
(44) Weigel, F.; Hauy, H. *Radiochim. Acta* **1965**, *4*, 327.
(45) Hobart, D. E.; Begun, G. M.; Haire, R. G.; Hellwege, H. E. *J. Raman Spectrosc.* **1983**, *14*, 59−62.
(46) Podor, R.; Cuney, M. *Am. Mineral.* **1997**, *82*, 765−771.
(47) Podor, R.; Cuney, M.; Nguyen-Trung, C. *Am. Mineral.* **1995**, *80*, 1261−1268.
(48) Podor, R.; François, M.; Dacheux, N. *J. Solid State Chem.* **2003**, *172*, 66−72.
(49) Muto, T.; Merowitz, R.; Pommer, A. M.; Murano, T. *J. Am. Mineral.* **1959**, *44*, 633−650.
(50) Feigelson, R. S. *J. Am. Ceram. Soc.* **1964**, *47*, 257−258.
(51) Kelly, K. L.; Beall, G. W.; Young, J. P.; Boatner, L. A. In *Scientific Basis for Nuclear Waste Management*; J. G. Moore: New York, 1981; Vol. 3, p 189.
(52) Mullica, D. F.; Sappenfield, E. L.; Wilson, G. A. *Lanthanide Actinide Res.* **1989**, *3*, 51−61.
(53) Montel, J. M.; Devidal, J. L. *EUG XI, Symposium PCM6*, Cambridge Publication, 680, 2001.
(54) Seaborg, G. T. In *Plutonium Chemistry*; W. T. Carnall, W. T.; Choppin, G. R., Eds.; American Chemical Society: Washington, 1983.
(55) Bamberger, C. E.; Begun, G. M.; Brynestad, J.; Land, J. F. *Radiochim. Acta* **1982**, *31*, 57−64.
(56) Dacheux, N.; Podor, R.; Brandel, V.; Genet, M. *J. Nucl. Mater.* **1998**, *252*, 179−186.
(57) Orlova, A. I.; Kitaev, D. B. *Radiochemistry* **2005**, *47*, 14−30.
(58) Tabuteau, A.; Pagès, M.; Livet, J.; Musikas, C. *J. Mater. Sci. Lett.* **1988**, *7*, 1315−1317.
(59) Orlova, M. P.; Orlova, A. I.; Gobechiya, E. R.; Kabalov, Y. K.; Dorokhova, G. I. *Crystallogr. Rep.* **2005**, *50*, 48−51.
(60) Heindl, R.; Flemke, E.; Loriers, J. *Conf. Dig. Inst. Phys.* **1971**, 222−224.
(61) Orlova, A. I.; Kitaev, D. B.; Volkov, Y. f.; Pet'kov, V. I.; Kurazhkovkaya, V. S.; Spiridonova, M. L. *Radiochemistry*, **2001**, *43*, 225−228.
(62) Pepin, G. J.; Vance, E. R.; McCarthy, G. J. *Mater. Res. Bull.* **1981**, *16*, 627−633.

ments.[63,64] Nevertheless, the authors did not determine the valence state of cerium in these powdered samples.

On the basis of such results, Podor et al. described the limit of incorporation of tetravalent element in brabantite samples, $M^{II}_{0.5}M^{IV}_{0.5}PO_4$, versus the ionic radius of divalent cation $\overline{^{IX}r(M^{II})}$, tetravalent cation $\overline{^{IX}r(M^{IV})}$, and the average cationic radius $\overline{^{IX}r(M^{IV+II})}$ in the nine-fold coordination through the following two relationships:[46,47]

$$1.107\ \text{Å} \leq \overline{^{IX}r(M^{IV+II})} \leq 1.216\ \text{Å} \quad (3)$$

$$1.082 \leq \overline{^{IX}r(M^{II})}/\overline{^{IX}r\,(M^{IV})} \leq 1.238 \quad (4)$$

which becomes:

$$1.107\ \text{Å} \leq \overline{^{IX}r(M^{III+IV+II})} \leq 1.216\ \text{Å} \quad (5)$$

$$1 \leq \overline{^{IX}r(M^{III+II})}/\overline{^{IX}r(M^{III+IV})} \leq 1.238 \quad (6)$$

with

$$\overline{^{IX}r(M^{III+IV+II})} = (1-2x)^{IX}r(M^{III}) + x^{IX}r(M^{II}) + x^{IX}r(M^{IV}) \quad (7)$$

and

$$\overline{^{IX}r(M^{III+II})}/\overline{^{IX}r(M^{III+IV})} = [(1-2x)^{IX}r(M^{III}) + x^{IX}r(M^{II})]/[(1-2x)\,^{IX}r(M^{III}) + x^{IX}r(M^{IV})] \quad (8)$$

when discussing the simultaneous substitution of trivalent lanthanide by divalent and tetravalent cations in monazite/brabantite solid solutions, $M^{III}_{1-2x}M^{II}_xM^{IV}_xPO_4$.

Both $\overline{^{IX}r(M^{IV+II})}$ and $\overline{^{IX}r(M^{II})}/\overline{^{IX}r(M^{IV})}$ values were determined from eqs 3 and 4, on one hand, and from the ionic radii of actinides determined according to Shannon,[65] on the other hand, with the assumption that the evolution of the actinide ionic size follows a linear function of the atomic number as well as in the eight-fold coordination.[16] These values reach 1.105 and 1.14 Å, 1.10 and 1.16 Å, and 1.09 and 1.17 Å for $Ca_{0.5}Np_{0.5}PO_4$, $Ca_{0.5}Ce_{0.5}PO_4$, and $Ca_{0.5}Pu_{0.5}PO_4$, respectively. On the basis of these results, the formation of $Ca_{0.5}Pu_{0.5}PO_4$ and $Ca_{0.5}Ce_{0.5}PO_4$ brabantites would be difficult since the $\overline{^{IX}r(M^{IV+II})}$ value does not satisfy the inequality given in eq 3, while that of $Ca_{0.5}Np_{0.5}PO_4$ and $Ca_{0.5}Np_{0.35}Pu_{0.15}PO_4$ remains possible, as described in the literature. In the same way, the maximum incorporation of the tetravalent actinide/element in $M^{III}_{1-2x}M^{II}_xM^{IV}_xPO_4$ was evaluated for M^{III} = La and M^{II} = Ca (Table 1). The coupled substitution $2Ln^{III} \leftrightarrow M^{IV} + M^{II}$ does not appear to be complete for cerium ($x_{max} = 0.47$) or plutonium ($x_{max} = 0.45$). Additionally, Zr and Hf could not be used as a surrogate for radioactive tetravalent elements ($x_{max} \approx 0.3$).

Table 1. Ionic Radii of Some Tetravalent Cations in the Nine-Fold Coordination and Their Maximum Incorporation in $LaPO_4$ ($La_{1-2x}M^{IV}_xCa_xPO_4$)

M^{IV}	Zr	Hf	Ce	Th	U	Np	Pu
$\overline{^{IX}r_{M(IV)}}$ (Å)	0.89	0.90	1.02	1.09	1.05	1.03	1.01
x_{max}	0.30	0.31	0.47	0.50	0.50	0.49	0.45

The aim of this paper is thus to investigate (re-examine) the incorporation of three tetravalent elements (Th, U, Ce) in the brabantite structure through the high-temperature solid-state route. In this work, thorium is considered on the basis of its stabilized tetravalent oxidation state, which excludes other redox reactions. In contrast, tetravalent uranium that can be oxidized and cerium (used as a plutonium surrogate) that can be reduced have been considered in a second part of the work. A particular aspect of this study consists of the description of the synoptic scheme of incorporation of these three tetravalent elements (Th, U, Ce) in the brabantite structure, as a preliminary work dedicated to the formation of monazite/brabantite solid solutions including tetravalent thorium and/or uranium.

2. Experimental Section

All the samples were prepared by firing initial mixtures containing MO_2, $Ca(HPO_4)\cdot 2H_2O$ (or CaO for cerium compounds), and $NH_4H_2PO_4$.[1,17] In order to increase the reactivity of the initial mixtures, the starting materials were ground for few minutes by mechanical grinding in zirconia bowls. Then they were fired under an inert atmosphere (M = Th, U) or in air (M = Ce) in alumina boats with heating and cooling rates of 10 °C·min^{-1}. In regards to the improvement of the final homogeneity of the samples, the optimization of the grinding conditions has already been described for several phosphate ceramics doped with thorium and/or uranium such as thorium phosphate−diphosphate solid solutions, britholites, monazites, and monazite/brabantite solid solutions.[7]

The thermal behavior of the mixtures was followed by differential thermal analysis (DTA) and thermogravimetry (TG) using a Setaram TG 92−16 apparatus in platinum crucibles. The X-ray diffraction diagrams were collected with a Bruker D8 Advanced Roentgen diffractometer system using Cu Kα rays (l = 0.15418 nm) from 5° to 60° (2θ) with the following data collection: 0.01°·step^{-1} and 2 s·step^{-1}. The precise peaks positions were determined using the fitting program *EVA*, available in the software package *Diffrac-AT*, version 3.0 (Socabim, France). The unit cell parameters were refined using the *U-Fit* or *PowderCell* software.[66,67]

The electron probe microanalyses (EPMA) experiments were carried out using the Cameca SX 50 and SX 100 apparatus (operating with an acceleration voltage of 15 kV and a current intensity of 10 nA). The calibration standards used were mainly $LaPO_4$ and $CePO_4$ monazites (Kα emission of phosphorus and Lα emission of cerium, respectively), wollastonite Ca_2SiO_4 (Kα emission of calcium), ThO_2 (Mα emission of thorium), and $UO_{2.12}$ (Mβ emission of uranium). It is worth noting that some interferences were detected during the EPMA analyses in the samples simultaneously containing large amounts of calcium and uranium, leading to the systematic overestimation of the calcium content, as already discussed for $Ca_9Nd_{0.5}U_{0.5}(PO_4)_{4.5}(SiO_4)_{1.5}F_2$ (uranium−britholites) samples.[3]

(63) Imanaka, N.; Masui, T.; Itaya, M. *Chem. Lett.* **2003**, *32* (4), 400−401.
(64) Sivakumar, V.; Varadaraju, U. V. *Bull. Mater. Sci.* **2005**, *28* (3), 299−301.
(65) Shannon, R. D. *Acta Crystallogr.* **1976**, *A32*, 751−767.
(66) Evain, M. *U-Fit Program*; Institut des Matériaux de Nantes: Nantes, France, 1992.
(67) Kraus, W.; Nolze, G. *J. Appl. Crystallogr.* **1996**, *29*, 301−303.

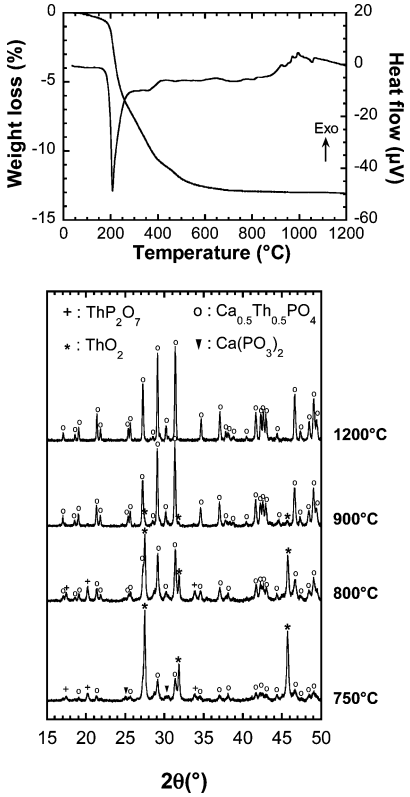

Figure 1. Thermal analysis under argon and XRD analysis of a ThO_2−$Ca(HPO_4)\cdot 2H_2O$−$NH_4H_2PO_4$ mixture versus the heating temperature.

The μ-Raman spectra were recorded with a microspectrometer LABRAM (Dilor, Jobin Yvon) using an argon laser operating at 514.5 nm with power in the range of 1−10 mW. The sample position was checked via an Olympus microscope.

Transmission electron microscopy (TEM) and electron energy loss spectroscopy (EELS) analyses were performed in the SACTEM-Toulouse facility, using a Tecnai F20 (FEI) instrument equipped with an objective lens aberration corrector (CEOS) and imaging filter (Gatan Tridiem).

3. Results and Discussion

3.1. Preparation of $Ca_{0.5}Th_{0.5}PO_4$. The synthesis of $Ca_{0.5}Th_{0.5}PO_4$ was followed versus the heating temperature ($400 \leq T \leq 1400$ °C) using DTA/TG experiments, from a starting mixture of $Ca(HPO_4)\cdot 2H_2O$, ThO_2 and $NH_4H_2PO_4$ (Figure 1).

The total weight loss observed on the TG curves (i.e., ≈13%) occurs in several steps below 600 °C. It was associated with the dehydration of $Ca(HPO_4)\cdot 2H_2O$ and to the decomposition of $NH_4H_2PO_4$. Between 180 and 400 °C, the total weight loss (≈10.8%) was associated with three endothermic effects located at 208, 360, and 474 °C, assigned to the release of water, to the condensation of hydrogenphosphate groups into polytrioxophosphate entities, and finally to the quantitative release of NH_3.[68] No additional weight loss is observed above 600 °C while several exothermic effects are observed at 777, 827, 925, 970, and 994 °C, due to reactions occurring between several intermediates, as discussed herein. Some of these peaks were globally associated to the formation then decomposition of thorium diphosphate (α-ThP_2O_7), calcium polytrioxophosphate ($Ca(PO_3)_2$), and to the formation of thorium−brabantite (i.e., $Ca_{0.5}Th_{0.5}PO_4$).

Table 2. EPMA Results of $Ca_{0.5}An_{0.5}PO_4$ Synthesized at 1200 °C for 6 h in Inert Atmosphere

	An = Th		An = U	
	obs	calc	obs	calc
wt % (O)	25.2 ± 0.2	27.7	28.3 ± 0.4	27.3
wt % (P)	14.0 ± 0.2	13.4	13.6 ± 0.2	13.2
wt % (Ca)	9.0 ± 0.1	8.7	9.3 ± 0.1[a]	8.6
wt % (An)	51.8 ± 0.6	50.2	51.5 ± 0.8	50.9
M/Ca	1.00 ± 0.02	1	0.94 ± 0.02[a]	1
P/(Ca + M)	1.01 ± 0.01	1	0.982 ± 0.008	1

[a] Interferences revealed during analyses, between uranium and calcium, leading to an overestimation of calcium.

The chemical reactions occurring during the formation of thorium−brabantite were also followed versus the heating temperature through XRD on samples heated at several temperatures ranging from 400 to 1400 °C (Figure 1). Between 400 and 700 °C, the XRD patterns always reveal the presence of ThO_2 (JCPDS file no. 42-1462) while the XRD lines of $Ca(HPO_4)\cdot 2H_2O$ and $NH_4H_2PO_4$ progressively disappear for the benefit of that of $Ca(PO_3)_2$ (JCPDS file no. 9-363) formed as an intermediate product. Above 750 °C, all the XRD lines of thorium−brabantite are observed (JCPDS file no. 31-311) as a consequence of the reaction between $Ca(PO_3)_2$ and ThO_2. Simultaneously, the XRD lines of α-ThP_2O_7 are also observed (JCPDS file no. 16-230). This intermediate progressively disappears above 900 °C. Between 800 and 900 °C, the system thus appears polyphase and consists of a mixture of $Ca_{0.5}Th_{0.5}PO_4$, $Ca(PO_3)_2$, ThO_2, and α-ThP_2O_7, between which several chemical reactions occur leading to the numerous effects observed during the DTA experiments. The thermal effects observed between 700 and 1000 °C are surely the consequence of several solid−solid reactions between all these compounds. Nevertheless, these effects cannot be easily discriminated, which contributes to some difficulties in their specific assignment, as already mentioned.

Above 1000 °C, the XRD patterns correspond to pure and single-phase thorium−brabantite,[69] of which the chemical composition is consistent with that expected (Table 2).

The spectroscopic characterization of $Ca_{0.5}Th_{0.5}PO_4$ through μ-Raman experiments confirms that all the vibration bands observed correspond to δ_S(P−O) (400−450 cm^{-1}), δ_{AS}(P−O) (530−650 cm^{-1}), ν_S(P−O) (≈980 cm^{-1}), and ν_{AS}(P−O) (1050−1150 cm^{-1}) associated to PO_4 entities as reported in Figure 2.

All the data recorded appear in good agreement with that reported in the literature.[70] Moreover, no vibration band associated to the P−O−P bridge characteristic of diphosphate entities or of polytrioxophosphate groups is observed (es-

(68) Abdel-Kader, A.; Ammar, A. A.; Saleh, S. I. *Thermochim. Acta* **1997**, *176*, 293−304.

(69) Montel, J. M.; Devidal, J. L.; Avignant, D. *Chem. Geol.* **2002**, *191*, 89−104.

(70) Podor, R. *Eur. J. Mineral.* **1995**, *7*, 1353−1360.

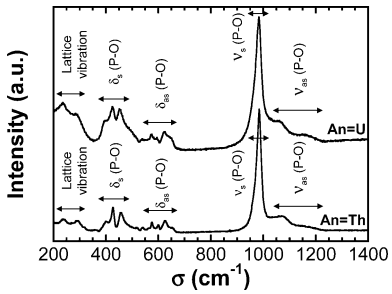

Figure 2. μ-Raman spectra of $Ca_{0.5}An_{0.5}PO_4$.

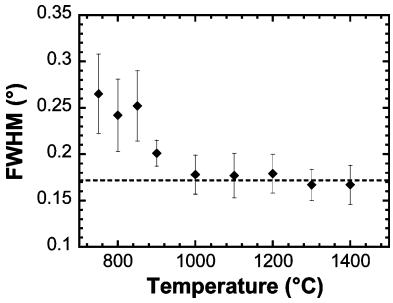

Figure 3. Average fwhm of the main XRD lines (i.e., $\bar{1}11$, $20\bar{1}$, 120, 012, $20\bar{2}$, and 112) of $Ca_{0.5}Th_{0.5}PO_4$ versus the heating temperature.

pecially in the range of 700−800 cm^{-1})[71] that confirms the complete reaction between intermediates such as α-ThP_2O_7 and $Ca(PO_3)_2$.

Finally, the crystallinity of the thorium−brabantite phase was followed through the determination of the average full width at half maximum (fwhm) of the main XRD lines, corresponding to the $\bar{1}11$, $20\bar{1}$, 120, 012, $20\bar{2}$, and 112 reflections (Figure 3), and of the refined unit cell parameters (Table 3).

From these data, it is clear that the crystallinity of thorium−brabantite samples is significantly improved when increasing the heating temperature from 750 to 1200 °C, the optimized conditions of preparation being obtained between 1200 and 1300 °C. At these temperatures, the unit cell parameters obtained (Table 3) appear in good agreement with the data reported in the literature for thorium−brabantite samples prepared through other chemical processes, which confirms the full incorporation of thorium in the monazite structure through the coupled substitution examined.[46,72] Finally, at 1400 °C, the powder X-ray diffraction data seems to indicate the beginning of the thermal decomposition of $Ca_{0.5}Th_{0.5}PO_4$, which was especially observed when increasing the heating time at this temperature. For higher heating temperatures, some small amounts of thorium dioxide were also detected at the surface of the samples (especially when working on thorium−brabantite pellets), as a consequence of the local decomposition of thorium−brabantite into calcium oxide, thorium dioxide, and volatile phosphorus oxide (P_4O_{10}), according to

$$Ca_{0.5}Th_{0.5}PO_4 \xrightarrow{T \geq 1400\ ^\circ C} {}^1/_2CaO + {}^1/_2ThO_2 + {}^1/_4P_4O_{10}\uparrow \quad (9)$$

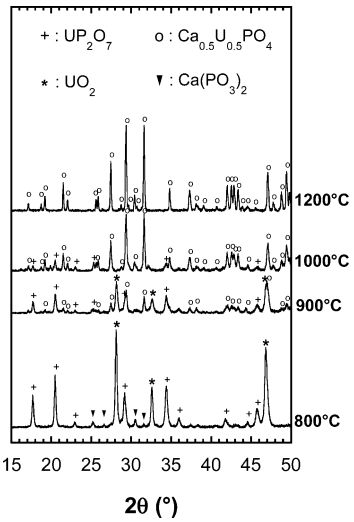

Figure 4. XRD analysis of a UO_2−$Ca(HPO_4)\cdot 2H_2O$−$NH_4H_2PO_4$ mixture versus the heating temperature.

3.2. Preparation of $Ca_{0.5}U_{0.5}PO_4$. From the results reported in the previous section, the full incorporation of thorium in the monazite structure appears possible when heating between 1200 and 1300 °C. However, as already discussed, thorium is expected to be only tetravalent in these operating conditions of synthesis. For this reason, the incorporation of uranium, which presents several stabilized oxidation states (mainly IV and VI in a phosphoric medium), was also examined. To this aim, mixtures of UO_2, $Ca(HPO_4)\cdot 2H_2O$, and $NH_4H_2PO_4$ were ground mechanically then fired at several heating temperatures ranging from 400 to 1400 °C.

The first indication of the progression of the solid−solid reaction was deduced from some changes in the color of the samples which turned from black/gray (due to the presence of UO_2 in the mixture) to green (characteristic of the presence of tetravalent uranium in phosphoric compounds)[73,74] when heating above 900 °C. Such an observation was correlated to the study of the variation of the XRD diagrams versus the heating temperature (Figure 4) which indicates that the incorporation of uranium in the monazite structure follows the same chemical scheme as that reported for thorium. Indeed, after the full dehydration of $Ca(HPO_4)\cdot 2H_2O$ then decomposition of $NH_4H_2PO_4$ between 100 and 600 °C, the XRD pattern emphasizes the presence of $Ca(PO_3)_2$ and α-UP_2O_7 (JCPDS file no. 16-263), as intermediates above 700 °C. All the XRD lines of uranium−brabantite ($Ca_{0.5}U_{0.5}PO_4$) are observed when heating above 900 °C, correlating to the decrease of the XRD lines of UO_2 (JCPDS file no. 41-1422). At this temperature, the $Ca_{0.5}U_{0.5}PO_4$ phase (JCPDS file no. 12-279) co-exists with UO_2 and α-UP_2O_7, which fully disappear at 900 °C and 1000 °C, respectively.

Pure and single-phase samples of uranium−brabantite are obtained when heating above 1100 °C. At this temperature, the elementary composition determined from EPMA appears

(71) Dacheux, N.; Brandel, V.; Genet, M. *New J. Chem.* **1995**, *19*, 15−25.
(72) Montel, J. M.; Glorieux, B.; Seydoux-Guillaume, A. M.; Wirth, R. J. *Phys. Chem. Solids* **2006**, *67*, 2489−2500.
(73) Bénard, P.; Louër, D.; Dacheux, N.; Brandel, V.; Genet, M. *Chem. Mater.* **1994**, *6*, 1049−1058.
(74) Dacheux, N.; Brandel, V.; Genet, M. *New J. Chem.* **1995**, *19*, 1029−1036.

Table 3. Unit Cell Parameters of $Ca_{0.5}M_{0.5}PO_4$ versus the Heating Temperature under an Ar Atmosphere

T (°C)	a (nm)	b (nm)	c (nm)	b (°)	$V \times 10^3$ (nm^3)	F_{20}
			M=Th			
Podor et al.[47]	0.6714	0.6921	0.6424	103.68	290.0	ND[a]
750	0.6728(4)	0.6918(3)	0.6432(3)	103.89(4)	290.6(4)	<10
800	0.6724(2)	0.6912(3)	0.6419(5)	103.94(4)	289.6(5)	13(0.0017;85)
900	0.6715(6)	0.6915(3)	0.6419(0)	103.79(7)	289.5(7)	73(0.0051;54)
1000	0.6711(8)	0.6915(5)	0.6417(0)	103.75(3)	289.3(5)	90(0.0054;41)
1100	0.6712(0)	0.6915(2)	0.6416(8)	103.73(7)	289.3(5)	89(0.0057;39)
1200	0.6712(3)	0.6916(9)	0.6416(3)	103.73(8)	289.4(5)	115(0.0051;34)
1300	0.6713(9)	0.6918(5)	0.6420(1)	103.73(7)	289.7(5)	103(0.0050;39)
1400	0.6713(7)	0.6918(1)	0.6418(7)	103.73(2)	289.6(5)	96(0.0055;38)
			M=U			
Montel et al.[69]	0.6673	0.6852	0.6364	104.07	282.3	ND
900	0.6675(2)	0.6853(2)	0.6372(2)	104.10(3)	283.0(2)	20(0.015;66)
1000	0.6672(8)	0.6859(0)	0.6373(3)	104.03(7)	283.0(2)	81(0.0039;63)
1100	0.6672(9)	0.6860(7)	0.6375(5)	104.03(6)	283.2(5)	92(0.0036;61)
1200	0.6672(4)	0.6860(1)	0.6376(6)	104.02(8)	283.2(6)	125(0.0039;41)
1300	0.6671(8)	0.6859(6)	0.6376(5)	104.02(5)	283.1(6)	70(0.0047;61)
1400	0.6670(6)	0.6860(7)	0.6378(2)	104.02(0)	283.2(5)	85(0.0041;57)

[a] ND: not determined.

in good agreement with that expected (Table 2), while the unit cell parameters determined (Table 3) seem to confirm the incorporation of tetravalent uranium in the monazite structure.[47]

The comparison of the μ-Raman spectra of $Ca_{0.5}Th_{0.5}PO_4$ and $Ca_{0.5}U_{0.5}PO_4$ does not reveal any significant differences (Figure 2). The positions of the vibration bands are very close, particularly the strong one located around 980 cm^{-1} (which can be assigned to ν_S(P−O) in phosphate groups). As for thorium−brabantite, it is worth noting that the vibrations usually associated to diphosphate or polytrioxophosphate groups are not observed, as a confirmation of the complete reaction of the intermediates formed at lower temperatures (α-UP_2O_7 or $Ca(PO_3)_2$). Moreover, the absence of an intense and narrow vibration band in the domain of 850−870 cm^{-1}, characteristic of the ν_1 symmetric stretching mode of uranyl units (UO_2^{2+}),[75−77] confirms the stabilization of tetravalent uranium during the entire synthesis process, which was suggested by the color of all the final samples prepared, as already discussed. These results contrast with that reported by McCarthy et al.,[78] who observed the oxidation of uranium(IV) during the heating treatment, and also with the data associated to the synthesis of uranium−britholites,[3] which revealed the formation of $CaUO_4$ then CaU_2O_{5+y} through a complex redox uranium cycle.

As observed for thorium−brabantite, the crystallinity of uranium−brabantite is significantly improved when increasing the heating temperature from 900 to 1200 °C (decrease of the average fwhm and improvement in the unit cell parameters refinement). The decomposition of uranium−brabantite begins above 1300 °C, leading to the formation of uranium dioxide (which can be evidenced by the change in color from green to gray/black). This decomposition is particularly observed at the surface of uranium−brabantite pellets, which are finally recovered by this thin black/gray uranium oxide layer when extending the heating time. As already discussed for thorium−brabantite, the associated reaction of decomposition can thus be written as

$$Ca_{0.5}U_{0.5}PO_4 \xrightarrow{T \geq 1300°C} {}^1/_2CaO + {}^1/_2UO_2 + {}^1/_4P_4O_{10}\uparrow \quad (10)$$

On the basis of the results obtained when studying the formation of thorium−brabantite and uranium−brabantite from mixtures of AnO_2 (An = Th, U), $Ca(HPO_4)\cdot 2H_2O$, and $NH_4H_2PO_4$, a simplified chemical mechanism can be proposed (Figure 5).

3.3. Synthesis of $Ca_{0.5}Ce_{0.5}PO_4$. As mentioned for uranium, plutonium could exist with two stabilized oxidation states (III and IV) in the phosphate environment. However, the trivalent oxidation state appears as the most favorable plutonium oxidation state in the monazite structure. Nevertheless, it is questionable if Pu(IV) could exist in such a structure when calcium is simultaneously incorporated. Because of the radiotoxicity of plutonium, experiments were first developed with cerium as a surrogate (since cerium presents similar properties with plutonium, both in terms of ionic size and redox properties). To this aim, the thermal behavior of a $CeO_2-CaO-2NH_4H_2PO_4$ mixture was investigated.

The physical and chemical phenomena occurring during the calcination of the starting mixture were followed through TG/DTA and XRD for $Ca_{0.5}Ce_{0.5}PO_4$ (Figure 6).

From room temperature to 800 °C, several thermal effects and an important weight loss were observed. All are assigned to the thermal decomposition of $NH_4H_2PO_4$ into NH_3 and H_2O, as previously observed for thorium (see Section 3.1). The observed weight loss (19.23%) matches well with that expected (19.22%). Beyond 800 °C, four thermal effects (930, 940, 946, and 1315 °C) and an additional weight loss (1.44% between 800 and 1050 °C) could be observed. With the TG derivative curve, not plotted on this graph, the latter can be assigned to the second endothermic effect occurring

(75) Frost, R. L.; Weier, M. L.; Martens, W.; Cejka, J. *Vib. Spectrosc.* **2006**, *41*, 205−212.
(76) Frost, R. L.; Weier, M. L. *Spectrochim. Acta* **2004**, *A(60)*, 2399−2409.
(77) Thomas, A. C.; Dacheux, N.; Le Coustumer, P.; Brandel, V.; Genet, M. *J. Nucl. Mater.* **2001**, *295*, 249−264.
(78) McCarthy, G. J.; White, W. B.; Pfoertsch, D. E. *Mater. Res. Bull.* **1978**, *13*, 1239−1245.

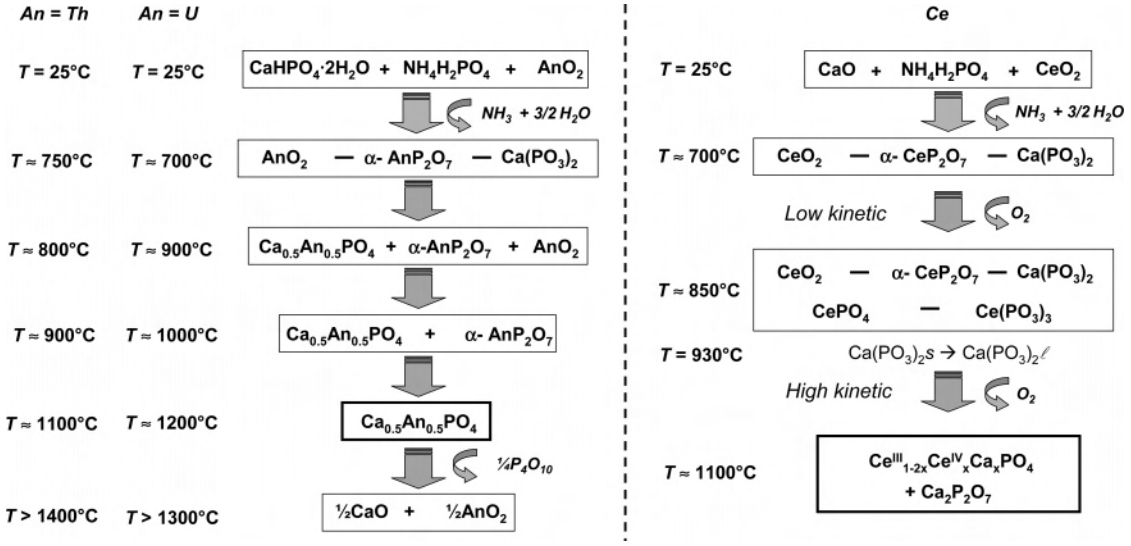

Figure 5. Thermal behavior of the starting mixture under an argon atmosphere (for Th and U) or in air (for Ce).

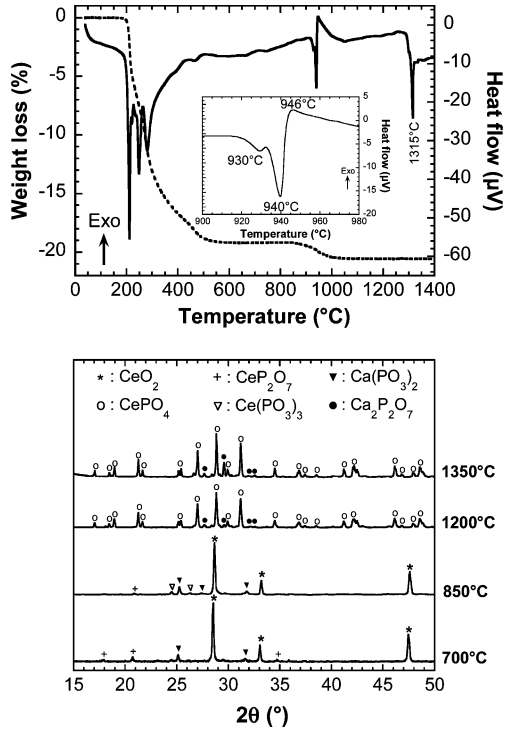

Figure 6. Thermal analysis under air and XRD analysis of a $CeO_2-CaO-2NH_4H_2PO_4$ mixture.

at 940 °C. The analysis of the emitted gas by mass spectrometry revealed that this weight loss is due to dioxygen emission. As already described for thorium and uranium, the XRD patterns revealed the presence of monazite and of calcium diphosphate $Ca_2P_2O_7$ (JCPDS file no. 73-0440), as previously described by Pepin et al.[62] Moreover, three other phosphates could be observed as transient compounds: CeP_2O_7 (JCPDS file no. 30-0164) and $Ca(PO_3)_2$ at 700 and 850 °C and $Ce(PO_3)_3$ (JCPDS file no. 33-0336) at 850 °C. Melting points of $Ca(PO_3)_2$ and $Ca_2P_2O_7$, measured by thermal analysis, were found to be located at 985 and 1318 °C, respectively. From these results, the qualitative mechanism of reaction can be proposed (Figure 5). The reactions can be sorted into two categories:

(a) Solid-state reactions (T < 930 °C). From 40 to 840 °C, the phosphate precursor melts and decomposes with emission of NH_3 and H_2O before reacting with CaO and CeO_2 to form $Ca(PO_3)_2$ and α-CeP_2O_7

$$2NH_4H_2PO_4 + CaO + CeO_2 \rightarrow Ca(PO_3)_2 + \alpha\text{-}CeP_2O_7 + 2NH_3\uparrow + 3H_2O\uparrow \quad (11)$$

From 840 to 930 °C, a slight weight loss is observed on the TG curve (Figure 6). According to the literature, this results in the slow decomposition of α-CeP_2O_7 as follows:[1,79,80]

$$2\alpha\text{-}CeP_2O_7 \rightarrow Ce(PO_3)_3 + CePO_4 + {}^1/_2O_2\uparrow \quad (12)$$

The oxygen emission appears as the consequence of the reduction of Ce(IV) into Ce(III).

(b) Liquid-state reactions (930 °C < T < 1050 °C). At 930 °C, $Ca(PO_3)_2$ melts (DTA effect at 930 °C) and dissociates into Ca^{2+} and PO_3^-:[81]

$$Ca(PO_3)_{2(s)} \rightarrow [Ca^{2+} + 2PO_3^-]_l \quad (13)$$

In such an ionic liquid, the Ce−O chemical bond of CeO_2 is probably broken.[81] Consequently, the liquid phase consists of four ions, i.e., $Ca^{2+} + 2PO_3^- + Ce^{4+} + O^{2-}$. Immediately, the kinetics of the reduction of Ce^{4+} strongly increases (DTA effect at 940 °C). Consecutively, a slow precipitation of two phases occurs (wide DTA effect at 946 °C) as

$$[Ca^{2+} + Ce^{3+} + 2PO_3^- + {}^3/_2O^{2-}]_l \rightarrow CePO_{4(s)} + {}^1/_2Ca_2P_2O_{7(s)} \quad (14)$$

(79) Botto, I. L.; Baran, E. J. *Z. Anorg. Allg. Chem.* **1977**, *430*, 283−288.
(80) Brandel, V.; Dacheux, N. *J. Solid State Chem.* **2004**, *177*, 4743−4754.
(81) Pascal, P. In *Nouveau Traité de Chimie Minérale*; Masson: Paris, 1956.

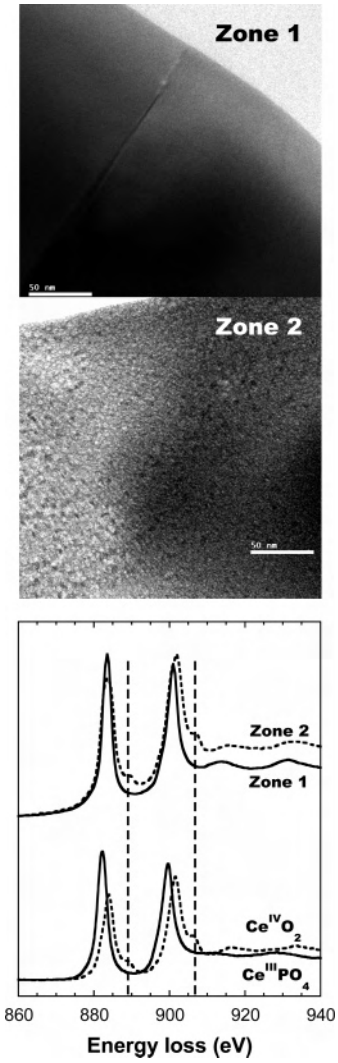

Figure 7. TEM observation and cerium EELS spectra of $M_{4,5}$-edge fine structure of $CeO_2-CaO-2NH_4H_2PO_4$ mixture heated at 1400 °C.

The DTA effect observed at 1315 °C can thus be assigned to the melting of $Ca_2P_2O_7$. In conclusion, the chemical reaction occurring during the calcination of the $CeO_2-CaO-2NH_4H_2PO_4$ mixture can be written as

$$CeO_2 + CaO + 2NH_4H_2PO_4 \rightarrow CePO_4 + {}^1/_2Ca_2P_2O_7 + 2NH_3\uparrow + 3H_2O\uparrow + {}^1/_4O_2\uparrow \quad (15)$$

with the assumption that this reaction is complete. However, several experiments indicate that the reaction reported in eq 15 is not complete and that the powder contains both trivalent and tetravalent cerium. The resulting powder exhibits a yellow-green color, as observed by Heindl et al.,[60] whereas $CePO_4$ is usually white colored. Moreover, the unit cell parameters are smaller ($a = 6.711(3)$ Å, $b = 7.036(4)$ Å, and $c = 6.384(0)$ Å) than those reported for pure $CePO_4$ ($a = 6.800$ Å, $b = 7.024$ Å, and $c = 6.474$ Å),[1] which appears in agreement with the partial incorporation of Ce(IV) in the monazite structure, since ${}^1/_2(Ce^{IV} + Ca^{II})$ is smaller than Ce^{III} (1.10 and 1.196 Å, respectively).[65] The presence of Ce^{IV} in the monazite structure was highlighted without any ambiguity by EELS (Figure 7).

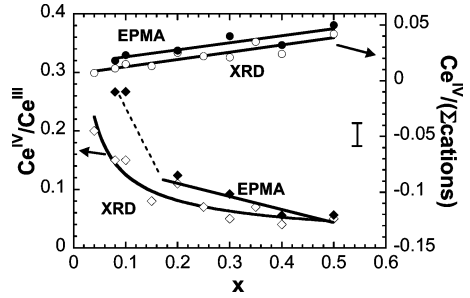

Figure 8. Variation of composition of the $La_{1-2x}Ce^{III}_{x-y}Ce^{IV}_yCa_y(PO_4)_{1-x+y}$ solid solution versus x.

Two different types of zones were observed by TEM. The first one appears with a uniform contrast and an amorphous structure (zone 1 in Figure 7), while in the second one, crystallized nanostructures were observed (zone 2 in Figure 7). The analysis of the fine structure of the cerium $M_{4,5}$-edge doublet leads to several remarks:

The spectra of zone 1 are characteristic of trivalent cerium; the shift of the doublet toward the high energies, the extra shoulders observed in zone 2 spectra, and the inversion of the intensity ratio between the two peaks prove the presence of Ce(IV) in this zone, in agreement with experiments performed on Ce^{III} and Ce^{IV} reference samples and with the literature.[82,83] Moreover, calcium is only detected in zone 2, which is consistent with the presence of Ce^{IV} in this zone.

3.4. Incorporation of Ce^{IV}/Ca^{II} in $(La,Ce)^{III}PO_4$ Solid Solution. The previous results have shown that only a small amount of tetravalent cerium could be incorporated in the monazite structure. Two hypotheses could explain this incomplete incorporation: Tetravalent cerium is unstable in monazite because of redox properties or the (Ce^{IV},Ca^{II}) couple is too small to incorporate the monazite structure. In that case, the incorporation should be linked to the global cationic size. Thus, the Ce^{IV}/Ce^{III} ratio should be higher in $LaPO_4$ than in $CePO_4$. Consequently, the incorporation of the (Ce^{IV},Ca^{II}) couple was investigated in the $LaPO_4-CePO_4$ solid solution as

$${}^1/_2(1-2x)La_2O_3 + xCeO_2 + xCaO + NH_4H_2PO_4 \rightarrow La_{1-2x}Ce^{III}_{x-y}Ce^{IV}_yCa_y(PO_4)_{1-x+y} + {}^1/_2(x-y)Ca_2P_2O_7 + NH_3\uparrow + {}^1/_2H_2O\uparrow + {}^1/_4(1-2x)O_2\uparrow \quad (16)$$

The measurement of the Ce^{IV}/Ce^{III} ratio was obtained by using two methods:

(a) EPMA experiments: In the monazite phase, the amount of tetravalent cerium was determined by measuring both Ca and Ce contents, noted (Ca) and (Ce), respectively, with the assumption that Ca^{2+} acts as the only charge compensation mechanism. The Ce^{IV}/Ce^{III} mole ratio is thus given by the following relationship:

$$\frac{Ce^{IV}}{Ce^{III}} = \frac{(Ca)}{(Ce)-(Ca)} \quad (17)$$

(82) Garvie, L. A. J.; Busek, P. R. *J. Phys. Chem. Solids* **1999**, *60*, 1943−1947.
(83) Colettan, M. *J. Mater. Sci. Lett.* **2002**, *21*, 1797−1801.

Table 4. Determination of the Ce^{IV}/Ce^{III} Mole Ratio in Monazite through XRD and EPMA

	XRD			EPMA			
x	$\overline{^{IX}r}$ (Å)	y	Ce^{IV}/Ce^{III}	(Ca)	(Ce)	y	Ce^{IV}/Ce^{III}
0.04	1.214 ± 0.001	0.007 ± 0.001	0.20 ± 0.01	0.018 ± 0.004	0.035 ± 0.008	0.02± 0.01	1.0 ± 0.7
0.06	ND	ND	ND	0.018 ± 0.002	0.04 ± 0.02	0.02 ± 0.01	0.6 ± 0.4
0.08	1.212 ± 0.001	0.010 ± 0.001	0.15 ± 0.01	0.018 ± 0.002	0.086 ± 0.008	0.017 ± 0.004	0.28 ± 0.10
0.10	1.211 ± 0.001	0.013 ± 0.001	0.15 ± 0.01	0.019 ± 0.002	0.091 ± 0.008	0.021 ± 0.005	0.27 ± 0.09
0.15	1.210 ± 0.001	0.011 ± 0.001	0.08 ± 0.01	ND[a]	ND	ND	ND
0.20	1.206 ± 0.001	0.020 ± 0.001	0.11 ± 0.01	0.027 ± 0.002	0.25 ± 0.04	0.022 ± 0.005	0.12 ± 0.04
0.25	1.205 ± 0.001	0.017 ± 0.001	0.07 ± 0.01	ND	ND	ND	ND
0.30	1.203 ± 0.001	0.015 ± 0.001	0.05 ± 0.01	0.040 ± 0.007	0.416 ± 0.02	0.029 ± 0.006	0.12 ± 0.04
0.35	1.198 ± 0.001	0.023 ± 0.001	0.07 ± 0.01	ND	ND	ND	ND
0.40	1.198 ± 0.001	0.015 ± 0.001	0.04 ± 0.01	0.040 ± 0.005	0.81 ± 0.07	0.020 ± 0.004	0.06 ± 0.02
0.50	1.188 ± 0.001	0.022 ± 0.001	0.05 ± 0.01	0.050 ± 0.007	0.95 ± 0.01	0.026 ± 0.004	0.06 ± 0.01

[a] ND: not determined.

The higher the (Ce) and (Ca) contents (i.e., for high x values), the more accurate the method. For the samples examined in this work, EPMA was not suitable for $x < 0.2$.

(b) XRD analysis: This method was based on the refinement of the unit cell parameters of the monazite phase from which it is possible to deduce the average cationic radius $\overline{^{IX}r(M^{III+II+IV})}$ considering, for instance, the following relation (where a represents the cell parameter):[1]

$$\overline{^{IX}r(M^{III+II+IV})} = \frac{a - 0.4718}{1.7420} \quad (18)$$

with

$$\overline{^{IX}r(M^{III+II+IV})} = \frac{(1-2x)^{IX}r_{La} + y^{IX}r_{Ce^{IV}} + y^{IX}r_{Ca^{II}} + (x-y)^{IX}r_{Ce^{III}}}{1-x+y} \quad (19)$$

which allows the determination of y according to

$$y = \frac{(1-2x)^{IX}r_{La} + x^{IX}r_{Ce^{III}} - (1-x)\overline{^{IX}r(M^{III+II+IV})}}{\overline{^{IX}r(M^{III+II+IV})} - {}^{IX}r_{Ce^{IV}} - {}^{IX}r_{Ca^{II}} + {}^{IX}r_{Ce^{III}}} \quad (20)$$

On the basis of the unit cell parameters determined, this method exhibits a constant accuracy, whatever the x value considered.

All the results reveal the presence of tetravalent cerium in monazite/brabantite samples (Table 4 and Figure 8). Nevertheless, the incorporation rate appears weak, i.e., $Ce^{IV}/(\Sigma \text{ cations}) < 10\%$, which is lower than the expected value (47%), deduced from sterical criteria (eqs 3−4 and Table 1).

Moreover, $Ce^{IV}/(\Sigma\text{cations})$ does not appear as a function of x. This highlights that the incorporation of the tetravalent form of an element in the monazite crystal structure is governed by the redox potential of the M^{4+}/M^{3+} couple with regard to O_2/O^{2-}. Unfortunately, the redox potentials of the M^{4+}/M^{3+} couples remain unknown in the conditions of synthesis considered. Nevertheless, it is possible to discuss on the basis of the values at 25 °C and 1 atm reported in aqueous solution.[84] In these conditions, the redox potential of Pu^{4+}/Pu^{3+} and Ce^{4+}/Ce^{3+} are close to that of O_2/O^{2-} (1.006 V/NHE, 1.72 V/NHE, and 1.12 V/NHE, respectively), which is in accordance with the existence of monazite containing both tri- and tetravalent cerium (this work) and plutonium.[16] Since the coexistence of M^{IV} and M^{III} in monazite is all the more important as the redox potential of the M^{4+}/M^{3+} couple is close to that O_2/O^{2-}, that can also easily explain why Pu^{IV} is incorporated in $LaPO_4$ at an higher level than Ce^{IV} ($M^{IV}/(M^{IV} + M^{III}) = 0.5$ for plutonium and 0.1 for cerium, respectively).

4. Conclusion

On the basis of the optimized grinding/heating conditions obtained for several phosphate-based ceramics, the full incorporation of tetravalent thorium or uranium in $Ca_{0.5}An_{0.5}PO_4$ samples occurred after heating at 1100and 1200 °C, respectively. At this temperature, pure and single-phase samples of brabantite are prepared, as confirmed by XRD and EPMA experiments.

In contrast, tetravalent cerium does not follow the same pattern. Indeed, its significant reduction at high temperature leads to the formation of cerium−monazite in the final polyphase systems obtained. The proportion of Ce(IV) is systematically lower than 10% of the total content of cations for all the samples prepared. This reduction, which is clearly associated to the release of dioxygen above 930 °C, can be also noted for tetravalent plutonium, as reported in another part of our study.

All these results confirm that a phosphoric medium appears necessary for reducing conditions in regard to elements and/or actinides, which usually leads to their reduction at their lower stabilized oxidation states, as already mentioned for several other actinide phosphate systems.[80,85] For these reasons, the incorporation of tetravalent thorium, uranium, and neptunium is easily reached while the formation of $Ca_{0.5}Ce_{0.5}PO_4$ and $Ca_{0.5}Pu_{0.5}PO_4$ is not favored by comparison to $CePO_4$ and $PuPO_4$ monazites.

Finally, the preparation of $Ca_{0.5}Th_{0.5-x}U_xPO_4$ and $La_{1-2x}Ca_xTh_{x-y}U_yPO_4$ was examined to simultaneously stabilize some trivalent and/or tetravalent actinides (i.e., minor actinides) in brabantites or in monazite/brabantite solid solutions. The optimization of the repetition of grinding/heating cycles required to get pure and homogeneous samples (especially

(84) Lide, D. R. *Handbook of Chemistry and Physics*, 73rd ed.; CRC Press: Boca Raton, FL, 1993.

(85) Brandel, V.; Dacheux, N. *J. Solid State Chem.* **2004**, *177*, 4755−4767.

pointing out the cation distribution in the solids) was examined. These results will be published in a following paper.

Acknowledgment. The authors are grateful to Johan Ravaux and Alain Kolher from LCSM (Université Henri Poincaré Nancy I, France) for performing EPMA and SEM experiments and to Thérèse Lhomme from CREGU (Université Henri Poincaré Nancy, I, France) for her extensive help during the characterization of the samples by the μ-Raman technique. This work was financially and scientifically supported by the French Research Group NOMADE (GdR 2023, CNRS/CEA/COGEMA) and by two CEA/CNRS research grants.

IC7012123